PHYSICAL REVIEW E **78**, 041602 (2008)

Hydrogen-terminated diamond electrodes. I. Charges, potentials, and energies

Jürgen Ristein, Wenying Zhang, and Lothar Ley
Technical Physics, University of Erlangen, Germany
(Received 25 March 2008; published 9 October 2008)

Hydrogen-terminated intrinsic diamond is a most unusual insulator since in contact with air or electrolyte it develops a hole accumulation layer just below the surface. When immersed in electrolyte the hole concentration responds to ionic charges and potentials and this response can be monitored by measuring the conductance of the hole accumulation layer without interference form the bulk conductivity. This feature has been widely used for chemical sensors in the form of solution-gate field effect transistors (SGFET). Here we analyze the charge and the potential profiles in the diamond and the electrolyte, as well as the static differential capacitance of the diamond electrode under controlled potential conditions. From this analysis we derive expressions for the transfer characteristics of diamond-based SGFET's that faithfully describe experimental data presented here as well. This holds in particular for the threshold region of the transfer characteristics that can only be modeled if the unusual semiconducting properties of the diamond electrode are taken into account properly. From fits to our data we derive (among other things) a value of $\chi=-0.50\pm0.02$ eV for the electron affinity of the hydrogen-terminated diamond surface in contact with aqueous electrolyte.

DOI: 10.1103/PhysRevE.78.041602 PACS number(s): 68.08.−p, 72.90.+y, 73.40.Mr

INTRODUCTION

Boron doped and hence conducting diamond has found application in waste water treatment and related electrochemical applications on account of its wide potential window that is second to none and allows for the reductive or oxidative destruction of noxious chemicals in a hydrous environment [1]. This is helped by the unsurpassed integrity of diamond against chemical and mechanical attack. Another promising application of diamond in this general area is that of ion sensitive field effect transistors (ISFET), that can be realized when an electrolyte takes the role of the gate contact between two ohmic source and drain contacts [solution gate field effect transistor (SGFET)] [2]. This application is usually based on the unique property of undoped diamond to acquire a pronounced surface conductivity (SC) that develops when the hydrogen terminated surface is exposed to humid air [3]. The surface conductivity amounts to about 10^{-6} S and is due to a hole accumulation layer with an areal density of the order of 10^{12} to 10^{13} cm^{-2} that is confined to the subsurface region by a self-imposed band bending [4]. Unlike band-bending-induced carrier accumulation at interfaces of certain semiconductor heterostructures, the holes are not accumulated from a solid-state phase; they are rather created in undoped diamond by an electrochemical reaction between the adventitious water layer on the diamond surface and diamond itself. As expounded by the charge transfer model of Maier *et al.* [3] a spontaneous redox reaction takes place at the interface whereby the diamond is oxidized and hydronium ions in the water layer are reduced to H_2. Later, Foord *et al.* [5] and Chakrapani *et al.* [6] suggested to consider the oxygen-hydroxyl redox couple as an alternative and no less plausible redox couple for the transfer doping reaction. We will focus on the redox activity of the hydrogen-terminated diamond surface and readdress the issue of active redox couples in a forthcoming presentation [7]. Unlike ignoble metals where similar redox reactions lead to the dissolution of the metal in the form of cations, in diamond the positive charge remains as free holes that are balanced by uncompensated anions in the water layer such as OH^- or HCO_3^-. The reason that the redox reactions take place spontaneously in diamond and not in other semiconductors lies in the fact that the ionization energy of a hydrogen terminated diamond surface, i.e., the distance from the valence band maximum (VBM) to the vacuum level, is as low as 4.2 ± 0.1 eV [8], i.e., lower than for any other semiconductor. The chemical potential, μ_{H_2}, for the H_3O^+/H_2 reaction when referenced to the vacuum level for a slightly acidic water layer (pH=5−7) and the very low concentration of dissolved hydrogen corresponding to the atmospheric partial pressure of 5.5×10^{-4} mbar [9] is -4.45 ± 0.06 eV. For the oxygen-hydroxyl redox couple an even lower value of $\mu_{O_2}=-5.30\pm0.06$ eV is found for atmospheric conditions (again pH=5−7 and O_2 partial pressure of 0.21 bar). Hence, as long as the Fermi level E_F in diamond lies above μ_{H_2} or μ_{O_2}, the redox reactions with the respective redox couple proceed and an upward surface band bending develops on account of the space charge of the accumulated holes. Under open circuit conditions, i.e., when the diamond surface is not involved in an electrochemical circuit fixing its potential, the electron exchange with the active redox couple(s) comes to a halt when the concentrations of the redox active species in the electrolyte and the holes at the diamond surface have adjusted such that the cathodic and the anodic currents across the diamond-electrolyte interface cancel [7].

The charm of this air-induced surface conductivity lies in the fact that it is readily turned into a field effect transistor (FET) of deceptively simple design as was first demonstrated by Kawarada *et al.* [10] and by Gluche *et al.* [11]. Two gold patches serve as ohmic contacts to the hole accumulation layer and constitute source (S) and drain (D) of the FET. A metal such as Al that forms a Schottky barrier on p-type diamond placed between source and drain repels holes and thus interrupts any current flow between S and D. When the Al gate is biased negatively, holes reaccumulate below the gate and the FET turns from off to on. Based on this prin-

 ©2008 The American Physical Society

ciple and, amazingly enough, without the necessity to provide an extra insulator between gate and channel, diamond-based FET's with excellent device performance have been realized [11,12].

Exploiting the exceptional chemical inertness of diamond and in addition its bio-compatibility, it is but a small step to turn the FET concept sketched above into an electrochemically active solution gate FET (SGFET), replacing the Al gate by an electrolyte and sensing any change in the electrolyte via changes in channel conductance. There has been considerable work in this direction over the last years that has culminated in the successful electrical detection of DNA hybridization taking place between single stranded DNA tethered to the diamond surface and a mixture of matching and nonmatching *s*-DNA in solution. For an up-to-date review we refer the reader to the articles by Nebel *et al.* [13,14].

When the control characteristics of an SGFET is sensitive to the ion composition of the electrolyte the device can be adopted as an ion sensitive field effect transistor (ISFET) for measuring ion concentrations, provided interference between different types of ions can be avoided. The simplest form of ion sensitivity is with respect to protons (or hydroxyl ions), i.e., the *p*H sensitivity of an SGFET. This *p*H sensitivity arises from the adsorption and desorption of protons at the diamond-electrolyte interface and leads to an increase of the channel conductivity with increasing *p*H value (positive *p*H sensitivity). The observation by a number of groups that a (reliable) *p*H sensitivity is usually only achieved after a slight anodic polarization of the electrode or upon partial oxidation or amination points to specific surface groups that participate in the protonation of the surface. Models of different complexity for this mechanism were proposed so far [2,15–18]. They are all based on the concept of a perfect polarizable diamond electrode, i.e., one that allows no faradaic current flow across the diamond-electrolyte interface.

Incorporating the hydrogen-terminated diamond surface in a SGFET configuration offers the possibility to study the charge and potential profiles at such an electrode in aqueous solution by using the channel sheet conductivity as a direct measurement of the areal hole density (aside from the carrier mobility as a scaling factor), i.e., of the surface charge of the electrode. This approach was first taken by Härtl *et al.* who measured the transfer characteristics (source-drain current vs source-gate voltage for constant source-drain voltage) to evaluate the ion adsorption at the diamond-electrolyte interface as a function of *p*H and ionic strength (KCl and $MgCl_2$) of the electrolyte [17]. Their data evaluation was based on the classical model of Grahame *et al.* for metal electrodes [19] and thus neglects the semiconductor character of the diamond electrode. Moreover, in their work the Galvani potential of the reference electrode was not considered which, implicitly and unnoticed, imposes a specific assumption on the electron affinity of the diamond electrode (see below). We will here follow the work of Härtl *et al.*, but will extend the classical Grahame model by taking the semiconductor character of the diamond electrode into account. In this work we have measured the SGFET characteristics of an intrinsic hydrogen-terminated diamond electrode for *p*H values between 2.4 and 7. The analysis will go beyond the classical Grahame model by including the idiosyncratic properties of the hole accumulation layer of the surface conductive diamond.

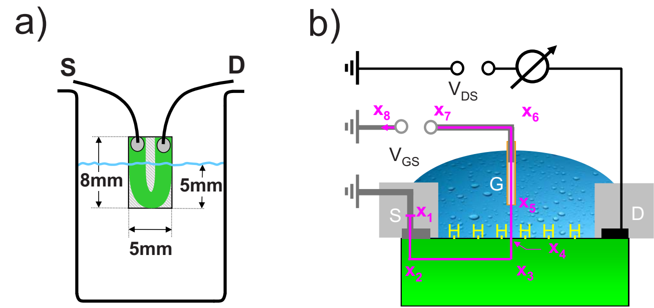

FIG. 1. (Color online) Schematics of the solution gate FET based on hydrogen-terminated surface conducting diamond. (a) Sample and contact geometry with the U-shaped, 2-mm-wide surface conductive channel; (b) the electrical circuit adopted in the experiment. All voltages are referenced to ground. The path from x_1 to x_8 is used in Fig. 5.

EXPERIMENT AND RESULTS

The sample used in this experiment is a natural type IIa single crystal diamond with (100) surfaces of 5 mm by 8 mm size. The sample was cleaned and hydrogen terminated following the recipe given in Ref. [20]. On the one side, a 2-mm-wide U-shaped surface conductive channel was defined by oxidizing the remainder of that surface as well as the edges and the back side of the sample in an oxygen plasma and thereby rendering those parts nonconducting [see Fig. 1(a)]. The channel is contacted at its ends by silver paste and gold wire leads which yields perfectly ohmic contacts that serve as source and drain. Care is taken that only the diamond surface and not the metal contacts are in contact with the electrolyte. This is achieved without any epoxy or sealant simply by dipping only the hydrogen-terminated diamond into the electrolyte and keeping the metal contacts out in air. Thus we obtain a conductive channel of about 16 mm length (source-drain distance) and 2 mm width. About 11 mm of the channel length are dipped into liquid and thus controlled over the whole cross section by the electrolytic gate [see Fig. 1(a)]. As a consequence, full pinch off of the channel is observed in the output characteristics of the FET (see below).

The electrolyte consists of 10 mM phosphate buffer and 10 mM KCl, which was titrated with H_3PO_4 and KOH to adjust the *p*H. All chemicals were purchased from Roth (Germany) and were used without further purification. The gate electrode is provided by an electrochemical Ag/AgCl reference electrode (3 M KCl solution) that was placed at a distance of 10 mm in front of the sample. We have chosen a double junction version to minimize contamination of the electrolyte (Schott B2220). The redox potential of that electrode is +0.20 V vs standard hydrogen electrode (SHE) at room temperature. The diamond electrode was grounded at the source contact and the gate voltage was applied to the gate electrode via a programmable voltage source. The cur-

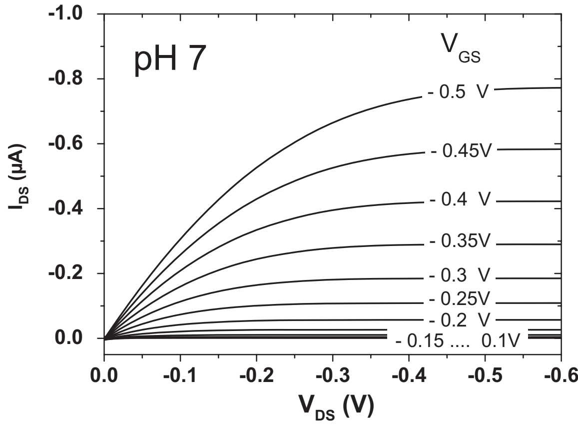

FIG. 2. Field effect output characteristics of the surface conductive diamond SGFET at a pH of 7.

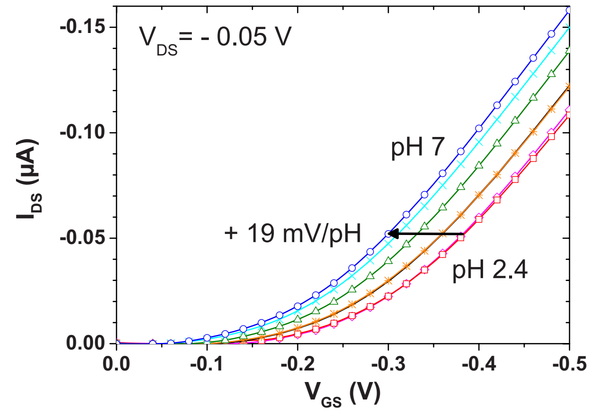

FIG. 3. (Color online) Transfer characteristics of the SGFET for a constant source-drain voltage of −0.05 V, i.e., in the linear I_{DS}-V_{DS} range. pH values are between 7 and 3 in steps of 1; the most acidic electrolyte has pH 2.4.

rent between diamond electrode and gate electrode corresponds to the gate current of the SGFET and was lower than 3 nA throughout our whole experiment. It was therefore unnecessary to use a three-electrode configuration with an extra counter electrode in the standard potentiostatic mode. The source-drain current was measured with a Keithley 617 electrometer. We use the same sign convention as other researchers in the diamond field as illustrated in the schematic electrical circuit of Fig. 1(b). All voltages are referenced to ground. This corresponds to the common use in solid-state electronics referring gate voltages to the source, but is opposite to the electrochemical convention referring working electrode potentials to the reference electrode. The gate current of the order of a few nA is due to the same redox reactions that are responsible for the generation of the hole accumulation layer according to the surface transfer doping model [3]. This redox activity is dealt with in detail in an accompanying paper by the same authors [7]. As a matter of fact, transfer currents of this order of magnitude account well for the times it takes to establish surface conductivity on diamond after exposure to air. In Fig. 2 the field effect output characteristics are shown for pH 7. The pH response of the SGFET is monitored as a change in the output characteristics such as the one shown in Fig. 2 when the proton concentration in the electrolyte is varied. When the drain-source voltage V_{DS} is kept constant at a value small compared to the pinch-off voltage, the drain-source current is proportional to the hole concentration in the FET channel. The transfer characteristics for a drain-source voltage of −0.05 V and pH values between 2.4 and 7 are shown in Fig. 3. Data points are represented by open symbols and the full lines are guides to the eye. For a constant source-gate voltage, increasing pH enhances the channel conductance. For a constant source-drain current, a change in pH results in a shift of the transfer characteristics on average by +19 mV/pH. For a set point of the ISFET of I_{DS}=−0.05 μA we have extracted the pH sensitivity from Fig. 3 as shown in Fig. 4. The straight line from a linear regression confirms the average pH sensitivity stated above. The value of 19±2 mV/pH is in good agreement with the one of 15 mV/pH recently reported by Dankerl *et al.* [18].

DISCUSSION

We will discuss the pH sensitive transfer characteristics of Fig. 3 by considering the potential diagram $w(x)$ of the complete electrochemical circuit as it is sketched in Fig. 5 along a path x defined in Fig. 1. It consists of (A from x_1 to x_4) the diamond electrode from source contact to the free surface exposed to the electrolyte; (B) the compact layer consisting of range 1 between the diamond surface and the inner Helmholtz plane (IHP) and of range 2 between the inner and the outer Helmholtz plane (OHP); (C, OHP to x_5) the diffuse layer in the electrolyte; (D, from x_5 to x_6) the gate electrode (Ag/AgCl) including its double layer towards the electrolyte and (E from x_7 to x_8) the gate voltage source. Note that in Ref. [17] the potential drop imposed by the reference electrode (its Galvani potential) and potential drop across the semiconductor section of the circuit (A) are missing and the inner and outer Helmholtz planes have been assumed to be identical (d_2=0). For reasons which will become obvious later we set the potential in the electrolyte where it is asymptotically constant to zero. Figure 5 is drawn as an electron band diagram and hence the potential $w(x)$ drawn as a bold

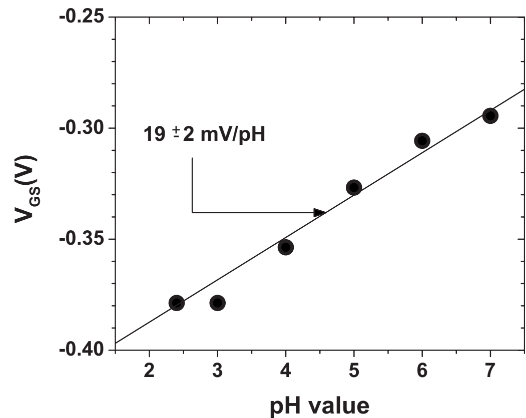

FIG. 4. The pH sensitivity of the SGFET in the limit of small source-drain current (V_{DS}=−0.05 V, I_{DS}=−0.05 μA) with the Ag/AgCl electrode used as gate electrode.

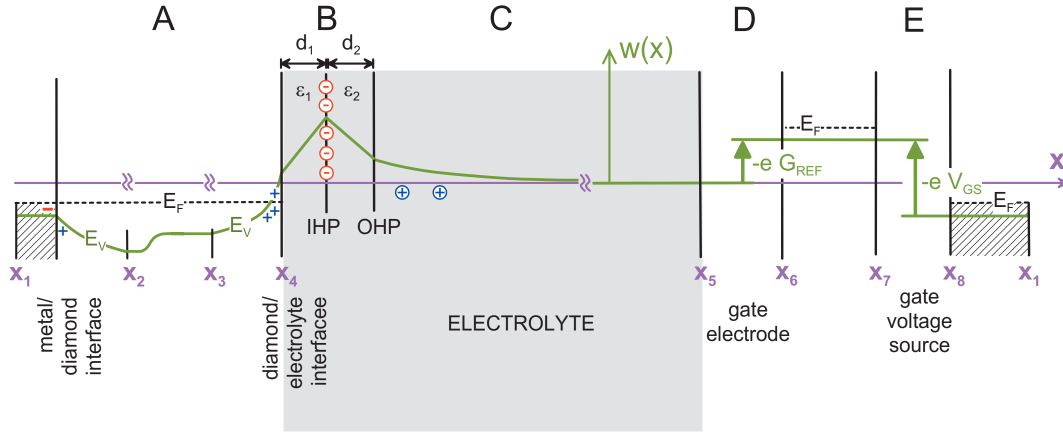

FIG. 5. (Color) The potential diagram $w(x)$ of the complete electrical source-gate circuit of the SGFET along the path depicted in Fig. 1. Between x_1 and x_2, and between x_3 and the axis break in range C, the diagram reflects a scale of the order of a few nanometers. In the other parts the diagram refers to macroscopic distances and only the discontinuities of the potential have been marked. Ionic charges in these parts are indicated as circles, electrons and holes just as minus and plus signs, respectively. For further details see text.

line refers to the electrostatic energy of a negative unit charge and has a sign opposite to that conventionally adopted in electrochemistry. In part A we choose the valence band maximum E_V to show the potential profile in the diamond. In the solid-state parts where the electrical current is carried by electrons (or holes), the Fermi level is indicated by a dashed line. The potential path inside of the diamond (metal-diamond interface to x_4) only serves to evaluate the potential drop between the diamond-electrolyte and the diamond-metal contact interface. The specific choice of this path is in fact arbitrary and not linked to the current or charge carrier profile in the diamond. The connection between potential and Fermi level is fixed at x_4 because there the total depth integrated areal hole density in the diamond accumulation layer p determines the position of E_V relative to E_F (see below) [4]. The gate voltage source results in the same discontinuity in both the electrostatic potential and the Fermi level between x_7 and x_8. The reference electrode creates a Galvani potential drop G_{REF} due to the equilibration of its characteristic redox couple with the electron reservoir of the solid. For simplicity we assume for the schematic of Fig. 5 that the metallic parts of the circuit are formed by only one material (i.e., silver). Different metals used in practice induce only contact potentials that cancel and need therefore not to be considered explicitly. The sheet charge σ_{ads} at the inner Helmholtz plane, that has been exemplary assumed to be negative in the potential diagram, is in general made up by two contributions: (i) Residual surface acceptors from the initial atmospheric doping process that do not equilibrate with the electrolyte when the sample is immersed from atmosphere into liquid, and (ii) preferentially absorbed ions from the electrolyte. Contribution (i) may or may not exist; contribution (ii) is the one usually held responsible for the ion sensitivity of the SGFET [17,21].

The relationship between the voltage applied to the gate, $V=\frac{1}{e}[w(x_8)-w(x_7)]$, and the areal hole density p in the diamond electrode, can best be understood by starting with a given hole density and constructing the associated band diagram including the voltage V_{GS}.

The areal hole density p defines the Fermi level at the diamond-electrolyte interface (x_4) relative to the valence band maximum E_V as described in detail in Ref. [4]. With the surface potential u_s at the diamond-electrolyte interface, $u_s=E_V-E_F$, the areal hole density p can be written as

$$p(u_s) = \sqrt{2kT\varepsilon\varepsilon_0 N_V/e^2}\,\exp\left(\frac{u_s}{2kT}\right) \tag{1a}$$

for the nondegenerate case ($u_s<0$) and

$$p(u_s) = \sqrt{2kT\varepsilon\varepsilon_0 N_V/e^2}\sqrt{1+\frac{u_s}{kT}+\frac{8}{15\sqrt{\pi}}\left(\frac{u_s}{kT}\right)^{5/2}} \tag{1b}$$

for the degenerate case ($u_s>0$).

$\varepsilon=5.8$ is the dielectric constant of diamond, ε_0 is the vacuum permeability, N_V is the effective valence band density of states of diamond which amounts to 2.7×10^{19} cm^{-3} at room temperature, e is the elementary charge, and kT is the thermal energy.

At the opposite boundary of part A of the circuit, i.e., at the metal-diamond interface, a corresponding interface potential u_{me} can be defined, again as the difference between E_V and the Fermi level. This interface potential is the result of the equilibration of electrons between the valence band of diamond and the metal and is given by the difference between the work function Φ_{me} of the metal and the ionization energy E_i of the diamond,

$$u_{me} = \Phi_{me} - E_i = \Phi_{me} - E_G - \chi. \tag{2}$$

In the last term on the right-hand side of (2) the ionization energy is alternatively expressed by the band-gap energy $E_G=5.5$ eV and the electron affinity χ of the hydrogen-terminated diamond. It is worth noting that u_{me} is independent of the ionic composition of the electrolyte and it is also independent of the applied voltage. The potential drop across the semiconductor part of the circuit is thus given as a function of p by inverting (1) and combining the result with (2):

$$w(x_4) - w(x_1) = u_s(p) - u_{me} = u_s(p) + E_i - \Phi_{me}. \tag{3}$$

We now turn to the potential profile across the electrolytic section of the circuit. The electric field E_1 (counted positive along $+x$ in Fig. 5) in the inner part of the compact layer, i.e.,

between x_4 and the IHP, is directly linked to the areal hole density by the Gauss law of electrostatics yielding $E_1 = ep/(\varepsilon_0\varepsilon_1)$, and it is modified by the adsorbed ion charge density σ_{ads} at the IHP to give $E_2 = (ep + \sigma_{ads})/(\varepsilon_0\varepsilon_2)$ for the outer part of the compact layer, i.e., between IHP and OHP. The dielectric constants ε_1 and ε_2 will in general deviate from that of the bulk electrolyte ($\varepsilon_{el} \approx 80$) on account of the restricted orientational freedom of the water molecules in the compact layer. Multiplying the electrical field with the respective spacings d_1 between x_4 and the IHP and d_2 between the IHP and the OHP gives for the potential drop across the compact layer

$$w_{OHP} - w(x_4) = \frac{ep}{\varepsilon_0\varepsilon_1} d_1 + \frac{ep + \sigma_{ads}}{\varepsilon_0\varepsilon_2} d_2. \quad (4)$$

Finally, the potential drop w_{OHP} across the diffuse layer is related to the depth-integrated areal ionic charge density $\sigma_{diff} = -ep - \sigma_{ads}$ in the diffuse layer by the Grahame equation [19]

$$\sigma_{diff} = -ep - \sigma_{ads} = \pm\sqrt{2\varepsilon_{EL}\varepsilon_0 RT}\sqrt{\left|\sum_{i=1}^{N} n_i^0 \left(e^{z_i w_{OHP}/(kT)} - 1\right)\right|}, \quad (5)$$

where the n_i^0 and the z_i are the asymptotic molar bulk concentrations and valencies, respectively, of the complete ensemble of ions in the electrolyte, and RT is the molar thermal energy—all quantities known for a given electrolyte [19]. The sign of σ_{diff} in Eq. (5) must be chosen identical to that of w_{OHP}. On the left-hand side we have used the overall charge neutrality condition for the complete diamond-electrolyte interface (including the hole accumulation layer) to link the diffuse layer ion charge density to the hole density.

In accordance with the approach taken by Härtl *et al.* [17] and others before, we assume that the sheet charge density σ_{ads} of ions affixed at the IHP depends on the electrolyte composition only (specifically on pH), but not on the potential w_{OHP}.

Although the Grahame equation looks quite complicated at first glance, it is easily seen that $|\sigma_{diff}(|w_{OHP}|, n_i^0)|$ is zero for $w_{OHP} = 0$ and is monotone increasing with all arguments. It can thus be inverted to yield $w_{OHP}(p, \sigma_{ads}) = w_{OHP} - w(x_5)$ where σ_{ads} is a constant parameter independent of the hole concentration, i.e., of the gate voltage.

The negative of the Galvani potential of the reference electrode $-eG_{REF} = w(x_6) - w(x_5)$ is the difference between the chemical potential μ_{Ag^+} of the redox electrons of the silver ions of the reference electrode and of the electrons in the metal phase of the reference electrode $\mu_{Ag} = -\Phi_{Ag}$, where we have alternatively expressed the chemical potential of the electrons in the solid silver phase relative to the vacuum level by the work function Φ_{Ag} of silver. Thus, $-eG_{REF} = \mu_{Ag^+} + \Phi_{Ag}$.

The last potential step in the circuit is provided by the gate voltage source, i.e., $w(x_8) - w(x_7) = eV_{GS}$. Kirchhoff's loop rule of electrostatics requires that all potential differences listed above add to zero. This yields the gate voltage V_{GS} that belongs to the hole density p,

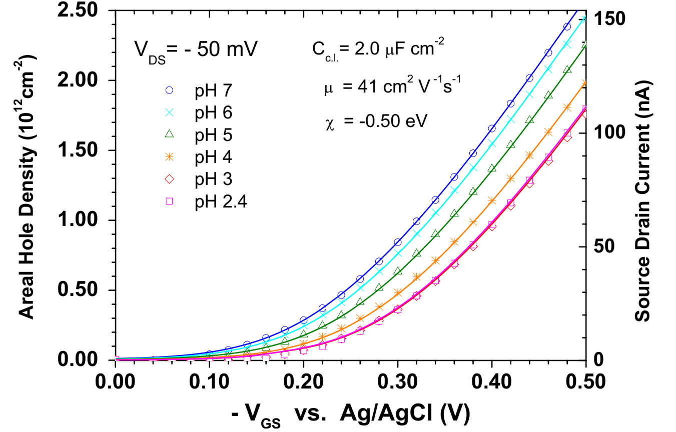

FIG. 6. (Color online) Fits of the transfer characteristics of Fig. 3 (symbols, right-hand scale) according to the model of Fig. 5 (hole densities on the left-hand ordinate). The parameter distinguishing the different pH cases is the adsorbed ionic charge density at the inner Helmholtz plane (IHP) as it is displayed in Fig. 8(a). Global parameters used in the model are the hole mobility ($\mu = 41$ cm^2 V^{-1} s^{-1}), the nominal areal capacitance of the compact layer (2.0 μF/cm^2), and the electron affinity of the hydrogen-terminated diamond surface in contact with the aqueous electrolyte ($\chi = -0.50$ eV).

$$-eV_{GS} = \frac{ep}{\varepsilon_0\varepsilon_1} d_1 + \frac{ep + \sigma_{ads}}{\varepsilon_0\varepsilon_2} d_2 - w_{OHP}(p, \sigma_{ads}) + \mu_{Ag^+} + \Phi_{Ag} - \Phi_{me} + E_i + u_s(p). \quad (6a)$$

The difference between the two metal work functions ($\Phi_{Ag} - \Phi_{me}$) is zero when Ag is used for the wiring of the circuit exclusively (assumed for the schematic of Fig. 5), or compensates with further contact potentials otherwise.

The chemical potential of the redox electrons associated with the silver ions of the reference electrode is $\mu_{Ag^+} = -4.44$ eV $- 0.20$ eV $= -4.64$ eV where we have used the energy of the standard hydrogen electrode (SHE) on the vacuum energy scale (-4.44 eV) and the redox potential of the reference electrode vs SHE ($+0.20$ eV). Thus, we finally have

$$eV_{GS} = (4.64 \text{ eV} - E_i) - u_s(p) - \frac{ep}{\varepsilon_0\varepsilon_1} d_1 - \frac{ep + \sigma_{ads}}{\varepsilon_0\varepsilon_2} d_2 + w_{OHP}(p, \sigma_{ads}). \quad (6b)$$

Equations (6) are essentially the inverse of the transfer characteristics shown in Fig. 3 and can directly be compared to the experimental values after using the geometry of the surface conductive channel, the hole mobility and the source-drain voltage to convert the source-drain current to the areal hole density. In Fig. 6 we have replotted the experimental data of Fig. 3 (symbols) and compare them with Eqs. (6) (solid lines). For each pH the correct ionic composition has been used to evaluate w_{OHP} for a given hole concentration according to Eq. (5). The ionic composition comprises monovalent and divalent positive and negative ions as it results from the buffer curves of the phosphate buffer, the titration, and the background salt concentration. The model

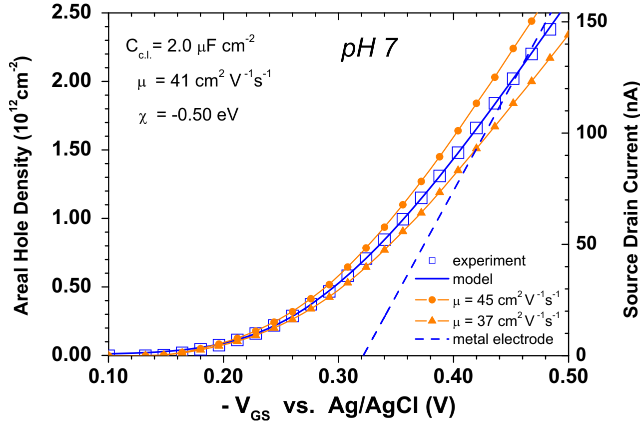

FIG. 7. (Color online) Fit of the transfer characteristics for pH7 with a variation of the mobility by $\pm 10\%$ around the optimum value of 41 $cm^2 V^{-1} s^{-1}$.

describes the data with excellent agreement in the superlinear threshold range and above. Following the work of Härtl *et al.* [17], we have set the inner and outer Helmholtz planes identical for this first scenario ($d_2=0$). That leaves $d_1/(\varepsilon_0\varepsilon_1)$ as the nominal inverse areal capacitance $1/C_{\text{c.l.}}$ of the compact layer as free parameter in (6). For the fits of Fig. 6(a) value of $C_{\text{c.l.}}$ of 2.0 μF/cm^2 was chosen. This value is the average of experimental values presented in [22,23]. We will readress the issue of the compact layer capacitance further below. Once the compact layer capacitance is fixed, the hole mobility of the carriers results with a small error margin from the fits of Fig. 6. This is demonstrated in Fig. 7 where we compare the transfer characteristics for pH7 with the fit for the optimum mobility μ=41 $cm^2 V^{-1} s^{-1}$ and for values deviating by $\pm 10\%$. All other parameters in (6), namely E_i and σ_{ads}, only shift the transfer characteristics on the voltage axes. It is thus obvious from Fig. 7 that the mobility is determined with an accuracy better than $\pm 10\%$ (once the compact layer capacitance is fixed).

The dashed line in Fig. 7 is the corresponding fit when the voltage drop across the diamond part of the electrical circuit is neglected, i.e., when Grahame's model for metal electrodes is adopted. It is obvious that the nonlinear transfer characteristics in the threshold range cannot be reproduced by the metallic model. The slope of the straight line is in that case (up to the elementary charge) identical to the areal capacitance of the compact layer as it is used as a fixed parameter in the model. However, it is apparent that the straight line does not follow the liear part of the transfer characteristics (source-drain current >100 nA). That means, an analysis of the transfer characteristics by the "metallic" model will underestimate the compact layer capacitance by 20%, all other parameters being equal.

Let us return to Fig. 6 for the discussion of the further parameters of the model. The shift of the transfer characteristics on the gate voltage axis is brought about by changes of the affixed ion charge density σ_{ads} which decreases with pH. The specific areal ion charge densities that are required for the fits in Fig. 6 are shown as a function of pH in Fig. 8(a) (full circles). They are essentially zero for pH 2.4 and 3 and become negative with increasing pH, reaching $\sigma_{\text{ads}}/e=-3\times 10^{13}$ cm^{-2} for pH7. Experimentally this charge density is inaccessible, but rather is the mobile ionic charge in the diffuse layer σ_{diff}. The latter is related to the potential w_{OHP} at the OHP by the Grahame equation (5). σ_{diff} changes complementary with the areal hole charge density and thus depends on the gate voltage. Under open circuit conditions w_{OHP} can be identified as the so-called ζ potential and extracted from streaming potential measurements. Open circuit conditions in a SGFET correspond to a situation where the source-gate voltage V_{GS} is equal to the open circuit voltage V_{OC} at the same diamond electrode measured versus Ag/AgCl under identical electrolyte conditions. From a fit of the experimental transfer characteristics to Eq. (6) a value of w_{OHP} for $V_{\text{GS}}=V_{\text{OC}}$ can be extracted which corresponds to the ζ potential. We have measured V_{OC} for pH between 2 and 10 [7] and the corresponding diffuse layer potential $-\frac{1}{e}w_{\text{OHP}}^{\text{OC}}$ vs pH is shown in (Fig. 8(b)) by the full circles.

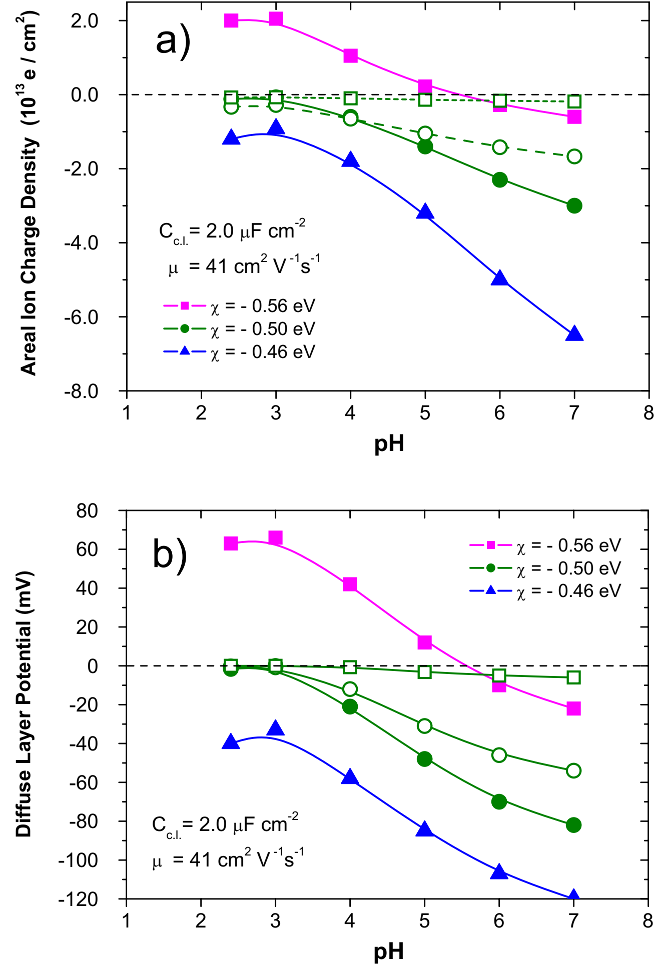

FIG. 8. (Color online) Areal ion charge density affixed at the IHP (a) and open circuit diffuse layer potential (b) as a function of pH as obtained from the fits of Fig. 6 (full circles) and from fits of the same accuracy but with different electron affinities χ (full squares and triangles). The open circuit diffuse layer potential can be identified with the ζ potential which is experimentally accessible by streaming potential measurements and which is found to be zero for pH$\approx$2–3.5. The open circles and open squares are the second and third scenarios, respectively. For details see the text.

Data on the ζ potential to be compared with $w_{\mathrm{OHP}}^{\mathrm{OC}}$ are so far only reported for a polycrystalline hydrogen-terminated diamond surface in contact with electrolytes comparable with the ones used here [6,17]. Since the sample used in that experiment was of high-quality material with presumably large grain sizes we consider the ζ potentials reported with some caveat also as representative for the case at hand. For a background salt concentration of 10 mM KCl comparable as in our case, the ζ potential varies from ≈ 0 mV at pH3 (the so-called isoelectric point) to ≈ -60 mV for pH7 which is in very good (albeit somewhat fortuitous) agreement with the data in Fig. 8(b) (0 to -80 mV).

From the comparison of the open circuit diffuse layer potentials $-\frac{1}{e}w_{\mathrm{OHP}}^{\mathrm{OC}}$ with the presented ζ potentials we can extract an important microscopic parameter of the hydrogen-terminated diamond surface in contact with aqueous electrolytes. To this end, we focus once more on Eqs. (6) that links the gate voltage to the hole density. It contains the difference between the diamond ionization energy E_i and 4.64 eV as an offset for the voltage axis. Thus, a change in the ionization energy (or—equivalently—of the electron affinity $\chi = E_i - 5.5$ eV) of the diamond surface causes a rigid shift of the transfer characteristics on the gate voltage axis. Such a shift can be compensated by appropriate changes in adsorbed ion densities σ_{ads} so that a fit as perfect as demonstrated in Fig. 6 is maintained. We have illustrated this compensation with three different assumptions for the electron affinity of the diamond surface. $\chi = -0.50$ eV is the case of Fig. 6 as discussed so far; $\chi = -0.56$ eV and $\chi = -0.46$ eV allow us to fit the transfer characteristics with the same accuracy (not shown). However, the corresponding open circuit diffuse layer potentials are far off the measured ζ potentials in those cases [Fig. 8(b)]. From this analysis we can thus determine the electron affinity of the hydrogen-terminated diamond (100) surface in contact with an aqueous electrolyte as $\chi = -0.50 \pm 0.02$ eV.

As mentioned above, the Galvani potential of the reference electrode and the voltage drop across the diamond electrode with the link to the diamond ionization energy are missing in the model in [17]. As is obvious from our discussion, this just corresponds to setting the offset, 4.64 eV$-E_i$, in Eq. (6b) equal to zero. This corresponds to the implicit assumption that the electron affinity of the diamond surface is $\chi = -0.86$ eV. The data presented in [17] are described reasonably well by using the Grahame model for metals in the linear range of the transfer characteristics. The parameter $\chi = -0.86$ eV that entered unintentionally and unnoticed in that work is significant and we must discuss the deviation of 0.36 eV of this value from the value χ inferred here.

Because E_i is just an additive factor to the gate voltage V_{GS} [see Eq. (6b)] any change in E_i causes a rigid shift of the transfer characteristics on the V_{GS} axis. The threshold voltages obtained from a linear extrapolation of the transfer characteristics serve as a measure for E_i independent of any modeling. For pH7, the data in [17] give a gate voltage of +0.20 V, whereas Fig. 3 yields -0.22 V, both using a Ag/AgCl reference electrode and both with an estimated uncertainty of about 10%. Literature data for the threshold voltage of hydrogen-terminated diamond SGFET's between pH7 and pH9 and for comparable ionic strengths as adopted in

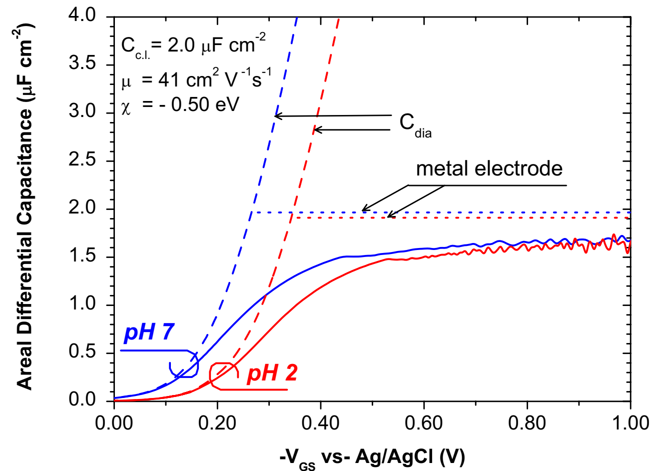

FIG. 9. (Color online) Areal differential capacitance of the complete circuit of Fig. 5 as extracted from the fits of Fig. 6 for pH2 and pH7. The noise on the curves is due to the numerical inversion of Eq. (1b).

our experiment and in [17] lie between -0.15 and -0.35 V when referenced to Ag/AgCl [2,16,24,25], thus never with positive polarity (The data of Ref. [24] were taken in 0.1 M H_2SO_4 vs a saturated calomel electrode.) We thus trust our data to be representative and consider the value of -0.50 eV determined for the electron affinity of the hydrogen-terminated diamond electrode in contact with aqueous electrolyte to be correct.

The derivative of the transfer characteristics of Fig. 3 constitutes the static differential capacitance for the total electrical circuit. We have extracted the areal differential capacitance from the fit curves to the data and show them for pH7 and pH2 in Fig. 9 (full lines). In the spirit of the model presented in Fig. 5 it is tempting to define $C_{\mathrm{dia}}(V_{\mathrm{GS}}) = e^2 \frac{dp(u_S)}{du_s}$ as the differential areal capacitance of the diamond accumulation layer alone (dashed lines in Fig. 9). This is so because $\frac{1}{e}u_s(p)$ mimics the modulation of the gate voltage-dependent potential drop across the hole accumulation layer [Eq. (1)]. The total capacitance is then a serial combination of C_{dia} and the double layer capacitance on the electrolyte side. In the threshold range of the transfer characteristics ($-V_{\mathrm{GS}} < 0.15$ V), the total areal capacitance is in fact dominated by C_{dia}, and it approaches a constant value in the linear range $-V_{\mathrm{GS}} > 0.5$ V. Note that this constant is, however, 20% lower than the nominal areal differential capacitance of the compact layer (2.0 μF cm^{-2}). Only when a metal electrode is modeled (horizontal dotted lines in Fig. 9), the capacitance of the whole circuit approaches that of the compact layer. The potential drop between the metal source contact and the diamond-electrolyte interface is thus the dominating effect for the static differential capacitance of the SGFET in the threshold range.

A final word needs to be said about the areal compact layer capacitance. In the scenario discussed so far, we have used a value of 2.0 μF/cm^2 consistent with experiment [22,18]. This value is about a factor of 8 lower than that of a compact layer as it is expected from its dielectric properties ($\varepsilon_1 \approx 6$, $d_1 \approx 0.25$ nm; $\varepsilon_2 \approx 30$, $d_2 \approx 0.35$ nm) and as it is

typically found on metal surfaces. The reason for this discrepancy is not understood at present. When only a consistent fit of the transfer characteristics shown above is aspired, a second scenario with a compact layer capacitance of $16\ \mu\mathrm{F/cm^2}$ works as well, however at the expense of a hole mobility reduced to $9.5\ \mathrm{cm^2\ V^{-1}\ s^{-1}}$. Essentially, in this second scenario the modulation of the SGFET channel conductivity is produced by larger concentration variations of less mobile holes. The adsorbed ion charge necessary to fit the pH dependence within this scenario and the resulting open circuit diffuse layer potentials (ζ potential) are plotted as open circles in Fig. 8. Within the uncertainty to be conceded they are also consistent with the pH dependence of the ζ potential reported in [17]. The electron affinity of the hydrogen-terminated diamond surface results as $\chi=-0.545$ eV in this scenario. This second scenario is motivated by testing the model outlined above with more plausible (as yet not measured) dielectric properties of the compact layer. We finally mention a third scenario with $d_1=0.25$ nm and $d_2=2.35$ nm with $\varepsilon_1=\varepsilon_2=6$. This gives an areal compact layer capacitance of $C_{\mathrm{c.l.}}=2.0\ \mu\mathrm{F\ cm^{-2}}$ consistent with experiment and with our fits. It allows a realistically close approach of the adsorbed ions to the surface and only requires to keep the hydrated mobile ions of the diffuse layer at comparatively large distance. Since $C_{\mathrm{c.l.}}$ is unchanged with respect to the first scenario, so is the hole mobility ($\mu=41\ \mathrm{cm^2\ V^{-1}\ s^{-1}}$). Due to the larger separation between the diffuse layer charge and the holes, the open circuit diffuse layer potential variation with pH (ζ potential sweep) is in this scenario only 6 mV between pH2 and pH7, i.e., about an order of magnitude smaller than measured experimentally [17]. The electron affinity determined in this third scenario is $\chi=-0.445$ eV.

We consider the first scenario discussed above the most realistic one since it is based on hole mobilities, differential capacitance values, and ζ potentials consistent with experiment. The second and third scenarios were motivated by the unusual dielectric properties of the compact layer that are not understood at present. If we consider them as extreme possibilities we may use the resulting electron affinities to specify a maximum uncertainty of $\Delta\chi\approx\pm0.05$ eV to a value extracted in the first scenario, giving altogether $\chi=-0.50\pm0.02$ eV for the electron affinity of the hydrogen-terminated diamond electrode in contact with aqueous solution.

ACKNOWLEDGMENT

This work was financially supported by the EU FP6 Marie Curie Research and Training Network "DRIVE" (Contract No. MRTN-CT-2004-512224).

[1] *Thin-Film Diamond II, Semiconductors and Semimetals*, edited by C. E. Nebel and J. Ristein (Elsevier/Academic, New York, 2004), Vol. 77, p. 121.
[2] H. Kawarada, Y. Araki, T. Sakai, T. Ogawa, and H. Umezawa, Phys. Status Solidi A **185**, 79 (2001).
[3] F. Maier, M. Riedel, B. Mantel, J. Ristein, and L. Ley, Phys. Rev. Lett. **85**, 3472 (2000).
[4] J. Ristein, J. Phys. D: Appl. Phys. **39**, R71 (2006).
[5] John S. Foord, Chi Hian Lau, Mineo Hiramatsu, Richard B. Jackman, Christoph E. Nebel, and Philippe Bergonzo, Diamond Relat. Mater. **11**, 856 (2002).
[6] Vidhya Chakrapani, John C. Angus, Alfred B. Anderson, Scott D. Wolter, Brian R. Stoner, and Gamini U. Sumanasekera, Science **318**, 1424 (2007).
[7] W. Zhang, J. Ristein, and L. Ley, Phys. Rev. E **78**, 041603 (2008), following paper.
[8] J. B. Cui, J. Ristein, and L. Ley, Phys. Rev. Lett. **81**, 429 (1998).
[9] NASA Earth Fact Sheet, http://nssdc.gsfc.nasa.gov/planetary/factsheet/earthfact.html
[10] H. Kawarada, M. Aoki, and M. Ito, Appl. Phys. Lett. **65**, 1563 (1994).
[11] P. Gluche, A. Aleksov, A. Vescan, W. Ebert, and E. Kohn, IEEE Electron Device Lett. **18**, 547 (1997).
[12] H. Umezawa, K. Tsugawa, S. Yamanaka, D. Takeuchi, D. Okushi, and H. Kawarada, Jpn. J. Appl. Phys., Part 2 **38**, L1222 (1999).
[13] C. E. Nebel, J. R. Soc., Interface **4**, 439 (2007).
[14] C. E. Nebel, B. Rezek, D. Shin, H. Uetsuka, and N. Yang, J. Phys. D: Appl. Phys. **40**, 6443 (2007).
[15] Jose A. Garrido, Andreas Härtl, Stefan Kuch, Martin Stutzmann, Oliver A. Williams, and R. B. Jackmann, Appl. Phys. Lett. **86**, 073504 (2005).
[16] H. Kanazawa, K. S. Song, T. Sakai, Y. Nakamura, H. Umezawa, M. Tachiki, and H. Kawarada, Diamond Relat. Mater. **12**, 618 (2003).
[17] Andreas Härtl, Jose A. Garrido, Stefan Nowy, Ralf Zimmermann, Carsten Werner, Dominik Horinek, Roland Netz, and Martin Stutzmann, J. Am. Chem. Soc. **129**, 1287 (2007).
[18] A. Dankerl, A. Reitinger, M. Stutzmann, and J. A. Garrido, Phys. Status Solidi (RRL) **2**, 31 (2008).
[19] D. C. Grahame, Chem. Rev. **41**, 441 (1947).
[20] M. Riedel, J. Ristein, and L. Ley, Phys. Rev. B **69**, 125338 (2004).
[21] Hirofumi Kanazawa, Kwang-Soup Song, Toshikatsu Sakai, Yusuke Nakamura, Hitoshi Umezawa, Minoru Tachiki, and Hiroshi Kawarada, Diamond Relat. Mater. **12**, 618 (2003).
[22] T. Kondo, K. Honda, D. A. Tryk, and A. Fujishima, Electrochim. Acta **48**, 2739 (2003).
[23] J. A. Garrido, S. Nowy, A. Härtl, and M. Stutzmann, Langmuir **24**, 3897 (2008).
[24] A. Denisenko, L. A. Kibler, and E. Kohn (private communication).
[25] J. A. Garrido, A. Härtl, S. Kuch, M. Stutzmann, O. A. Williams, and R. B. Jackmann, Appl. Phys. Lett. **86**, 073503 (2005).